THE ASTRONOMICAL JOURNAL, 121:2301–2307, 2001 May

A DEEP MULTICOLOR SURVEY. VII. EXTREMELY RED OBJECTS AND GALAXY FORMATION[1]

PAUL MARTINI[2]
Department of Astronomy, Ohio State University, 140 West 18th Avenue, Columbus, OH 43210-1173
Received 2000 September 19; accepted 2001 January 31

ABSTRACT

Extremely red objects (EROs) offer a window to the universe at $z \sim 1$ analogous to that provided by the Lyman break galaxies at $z = 3$. Passive evolution and hierarchical galaxy formation models make very distinct predictions for the K (2.2 μm) surface density of galaxies at $z \sim 1$, and EROs are a powerful constraint on these theories. I present a study of nine resolved EROs with $R-K \geq 5.3$ and $K \leq 18$ mag found in the 185 arcmin^2 of the Deep Multicolor Survey with near-infrared imaging. Photometric redshifts for these galaxies show they all lie at $z = 0.8$–1.3. The relatively blue $J-K$ colors of these galaxies suggest that most are old elliptical galaxies rather than dusty starbursts. The surface density of EROs in this survey (>0.05 arcmin^{-2}), which is a lower limit to the total $z \sim 1$ galaxy surface density, is an order of magnitude below the prediction of passive galaxy evolution, yet over a factor of 2 higher than the hierarchical galaxy formation prediction for a flat, matter-dominated universe. A flat, Λ-dominated universe may bring the hierarchical galaxy formation model into agreement with the observed ERO surface density.

Key words: cosmology: observations — galaxies: evolution — galaxies: formation — galaxies: photometry

1. INTRODUCTION

The best-known modern method of using color selection to find high-redshift galaxies is the Lyman break technique (e.g., Steidel & Hamilton 1993), and this method has isolated large numbers of galaxies at $z \sim 3$ and $z \sim 4$ (Steidel et al. 1996; Steidel et al. 1999). The great efficiency of the Lyman break technique in selecting high-redshift candidates for follow-up spectroscopy from visible wavelength colors has made it easier to preselect samples of $z \sim 3$ galaxy candidates than galaxies at $z \sim 1$–2. A complementary technique to preselect $z \sim 1$ galaxy candidates is to use a combination of near-infrared (NIR) and visible wavelength photometry to search for extremely red objects (EROs), which have large visible–NIR colors (Elston, Rieke, & Rieke 1988; McCarthy, Persson, & West 1992).

A sample of galaxies at $z \sim 1$ can test galaxy evolution theories by measuring both the surface density of these galaxies and the relative fraction of different spectrophotometric types. Hierarchical galaxy formation predicts that present-day massive galaxies assemble between $z \sim 1$ and the present (e.g., White & Rees 1978; White & Frenk 1991; Lacey et al. 1993; Baugh et al. 1998). In contrast, the passive evolution model postulates that galaxies assembled at $z > 3$ and the comoving space density of bright galaxies at $z \sim 1$ should be comparable to the local value (e.g., Tinsley 1977; Bruzual & Kron 1980). Kauffmann & Charlot (1998) showed that hierarchical galaxy formation predicts a significantly smaller fraction of $z \sim 1$ galaxies in a K-selected redshift survey relative to passive galaxy evolution. K-band selection is particularly sensitive to differences between these two galaxy formation models because it measures the old stellar population that dominates the mass, rather than recent starbursts that may enhance the luminosity at visible wavelengths. Several K-selected redshift surveys have indeed found smaller numbers of $z \geq 1$ galaxies than the number predicted by passive evolution, which supports the hierarchical galaxy formation picture (Songaila et al. 1994; Cowie et al. 1996; Fontana et al. 1999).

Well-studied EROs to date are all at $z \geq 0.8$ and appear to be either old elliptical galaxies or dusty starbursts. However, EROs are generally classified as elliptical galaxies because their rest-frame visible spectrum is dominated by an old stellar population, rather than on the basis of kinematic or surface brightness criteria. Old elliptical galaxies at these redshifts have very red colors because the 4000 Å break falls between the R and K bands. Dusty starbursts have similarly extreme colors due to a combination of the Balmer continuum break and the relative suppression of the UV light from young stars by dust. The first deep sky survey at K by Elston et al. 1988 found two EROs, which additional photometry and spectroscopy showed were old elliptical galaxies at $z = 0.8$ (Elston, Rieke, & Rieke 1989). Several more EROs were found by McCarthy et al. (1992) in a K imaging survey of the fields of high-redshift radio galaxies, and two EROs were found by Hu & Ridgway (1994) in an imaging survey of a $z = 3.790$ quasar field. One of these, HR 10, has a spectroscopic redshift of $z = 1.44$ and has since been detected at radio (Graham & Dey 1996) and submillimeter (Cimatti et al. 1998; Dey et al. 1999) wavelengths. These observations provide strong evidence that HR 10 is a dusty starburst galaxy. Another well-studied ERO, LBDS 53W091, was discovered in a NIR study of a sample of weak radio sources. Spectroscopy by Spinrad et al. (1997) showed that it is an old, red galaxy at $z = 1.55$. Soifer et al. (1999) observed the ERO Cl 0939+4713B, serendipitously discovered by Persson et al. (1993), and found it is an old elliptical galaxy at $z = 1.58$. The spectroscopic observations of HR 10, LBDS 53W091, Cl 0939+4713B, and others show that EROs are at $z \geq 0.8$ and are either old elliptical galaxies or dusty starbursts.

The definition of an ERO is highly variable and cuts in color include $R-K \geq 5$, 5.3, and 6 and $I-K \geq 4$. Recent

[1] Based on observations obtained at MDM Observatory, operated by Columbia University, Dartmouth College, the University of Michigan, and the Ohio State University.

[2] Current address: Carnegie Observatories, 813 Santa Barbara Street, Pasadena, CA 91101; martini@ociw.edu.

surveys for EROs have mapped large areas of the sky at NIR wavelengths to study the ERO population statistically (Thompson et al. 1999; Yan et al. 2000; Scodeggio & Silva 2000; Daddi et al. 2000). Cimatti et al. (1999) spectroscopically followed up a sample of nine EROs and found that two are dusty starbursts and the remaining seven are consistent with passively evolved elliptical galaxies. Cohen et al. (1999) have obtained spectra of four of the 19 EROs in the Caltech Faint Galaxy Redshift Survey, and all appear to be elliptical galaxies with little dust. This spectroscopic work indicates that most EROs are elliptical galaxies rather than dusty starbursts. While the larger ERO samples include only imaging, Daddi et al. (2000) showed that the EROs in their 700 arcmin^2 survey are strongly clustered and that their surface density can be used to test galaxy formation models. The clustering of EROs helps to explain the dispersion in measurements of the ERO surface density for a fixed color and magnitude threshold.

This survey for EROs is based on the visible and NIR imaging of the Deep Multicolor Survey (DMS) described in Hall et al. (1996a) and Martini (2001). The original DMS included $UBVRI_{75}I_{86}$ photometry of six high galactic latitude fields over a total area of 0.83 deg^2. The DMS has been used to study the luminosity function of quasars (Hall et al. 1996b; Kennefick et al. 1997), galactic stars (Martini & Osmer 1998), the luminosity function of galaxies (Liu et al. 1998), and NIR JHK number counts (Martini 2001). In this paper I discuss the nature of the nine objects with $R-K \geq 5.3$ and $K \leq 18$ mag in the DMS and the implications of the ERO surface density for galaxy evolution models. Sections 2 and 3 briefly describe the photometry and object selection. In § 4 I use colors and model fits to the nine-filter spectral energy distributions (SEDs) to compute redshifts and classify the EROs as either elliptical galaxies or dusty starbursts. These results are discussed in § 5.

2. PHOTOMETRY

The observations, data reduction, and photometric solutions for these observations are described in Hall et al. (1996a) and Martini (2001). To measure the objects detected in the NIR frames (plate scale 0.″3 pixel^{-1}) on the CCD data (0.″529 pixel^{-1}), I used the DMS stellar catalog (Osmer et al. 1998) to solve for the coordinate transformations using GEOTRANS in IRAF.[3] The photometric zero points for each of the 21 fields was determined with the DMS stellar catalog for the CCD images, and the photometric solutions were taken from Martini (2001) for the NIR images. Because the subfields with NIR data are small, variations in the point-spread function across the CCD fields described by Hall et al. (1996a) are negligible over these individual subfields. For the CCD fields with more than one NIR subfield, the variation in the photometric zero point for different regions of the same CCD image was 0.02 mag or less.

I measured the brightness of each object using aperture photometry and a stellar profile aperture correction. The main purpose of these measurements is to determine accurately the colors of the galaxies rather than their total integrated brightness in each filter. The same size aperture will sample the same physical region in each galaxy and provide a better estimate of the shape of the SED than methods such as isophotal magnitudes, which depend on the isophotal limit in each filter. Variations in seeing from filter to filter can complicate this issue, as a larger fraction of the light within a fixed physical radius falls outside the aperture if the seeing FWHM is larger. The optimal aperture for these measurements is a compromise between a decrease in aperture size, which increases the signal-to-noise ratio, and an increase in the uncertainty of the stellar aperture correction. While the image quality is on average superior in the NIR frames relative to the CCD data, the NIR fields are significantly smaller (9 arcmin^2 compared with 225 arcmin^2) and generally have only one or two stars of sufficient brightness to determine the seeing and aperture correction. The NIR frames were therefore the limiting factor in minimizing the aperture size. To derive the optimal aperture I measured the aperture correction in the NIR frames at a range of radii from 0.″5 to 4″. I found that for $R < 2''$ the uncertainty in the aperture correction for many of the frames was comparable to or greater than the photometric errors at $K \sim 18$ mag. I therefore chose to use an $R = 2''$ aperture for the photometry.

To measure the amount of lost light from a galaxy in excess of the stellar aperture correction, I simulated measurements of exponential disks and $r^{1/4}$ profiles with half-light radii $r_h = 0.''25$, 0.″5, 0.″75, and 1″ over the range of seeing from 1″ to 2.″5 FWHM exhibited by these images following the procedure described in Martini (2001). This range of possible ERO angular sizes spans that found by Moriondo, Cimatti, & Daddi (2000) in their study of EROs with *HST* imaging. For an $R = 2''$ aperture, the galaxy light lost in addition to the stellar aperture correction ranges from essentially zero for $r_h = 0.''25$ to 0.2 mag for an $r_h = 1''$ exponential disk and 0.25 mag for an $r_h = 1''$, $r^{1/4}$ profile.

3. SELECTION CRITERIA

NIR imaging surveys for EROs have defined numerous selection criteria (Thompson et al. 1999; Yan et al. 2000; Scodeggio & Silva 2000), including objects with $R-K \geq 6$, $R-K \geq 5$, $I-K \geq 4$, and K-magnitude upper limits from 18 to 20 mag. An extreme red color is a fairly efficient means of selecting candidate galaxies at $z \sim 1$ because it brackets the 4000 Å break in elliptical galaxies and the Balmer continuum plus reddening in dusty starburst galaxies. This color space could also be inhabited by late-type stars, emission-line galaxies, or very high redshift ($z > 7$) galaxies, where the Lyman continuum falls between R and K. Stellar contamination is probably the dominant contaminant in ERO samples and can be avoided by including only resolved sources. The upper limit in magnitude, which is approximately the spectroscopic limit of the largest current telescopes, avoids "contamination" of the $z \sim 1$ sample by galaxies at higher redshift, as they have much lower surface densities than $z \sim 1$ objects at these magnitude limits. For example, a $K = 18$ mag galaxy at $z = 1$ has an absolute magnitude $M_K = -25 + \log h$ (for $\Omega_M = 0.3$ and $\Omega_\Lambda = 0.7$), 2 mag brighter than $M_{*,K}(z = 0) = -23 + \log h$ (Gardner et al. 1997). The $z \geq 0.8$ galaxies in a survey to $K \sim 18$ mag will therefore mostly be at $z < 2$ because of the exponential decline in the galaxy luminosity function.

For this study I have adopted $R-K \geq 5.3$ and $K \leq 18$ mag to select for EROs in the DMS sample. The $K \leq 18$

[3] IRAF is distributed by the National Optical Astronomy Observatories, which are operated by the Association of Universities for Research in Astronomy, Inc., under cooperative agreement with the National Science Foundation.

mag limit is brighter than at least the $r_h = 0''.25$ completeness limit for nearly all 185 arcmin^2 of the K survey (Martini 2001). $R-K \geq 5.3$ was suggested by Pozzetti & Mannucci (2000), based on models of elliptical galaxies and dusty starbursts, as well as observations of known EROs at $z \sim 1$. In total, nine resolved objects in the DMS sample met these two selection criteria for a surface density of 0.05 arcmin^{-2}. This surface density is a lower limit due to the variation in detection efficiency for different galaxy sizes and from field to field. The photometry for the EROs is listed in Table 1. The only correction that has been applied to the apparent magnitudes in Table 1 is a stellar aperture correction. As these measurements may underestimate the total integrated brightness, this survey may underestimate the true ERO surface density (see § 5).

4. ANALYSIS

4.1. *ERO Colors*

Colors are one means of breaking the degeneracy between elliptical galaxies and starbursts. The SED of an elliptical galaxy at $z \sim 1$ drops off sharply at the 4000 Å break between the R and K bands, while the SED of a dusty starburst declines more gradually because of reddening. As discussed by Pozzetti & Mannucci (2000), observations between the R and K bands, such as I, z, J, or H can be used to measure the sharpness of the spectral break and thus discriminate between these two scenarios. By this argument, elliptical galaxies appear bluer in $J-K$ than dusty starbursts. Figure 1 shows $R-K$ versus $J-K$ for the galaxies in Table 1 (shown as open circles in Fig. 1), where elliptical galaxies lie to the left, toward bluer $J-K$ colors, and dusty starbursts lie to the right, toward redder $J-K$ colors. Pozzetti & Mannucci (2000) convolved a range of models and observed galaxy spectral energy distributions with R, I, J, and H filters and found that elliptical galaxies and dusty starbursts separate in the $I-K$ versus $J-K$ plane and the $R-K$ versus $J-K$ plane. Their relation between $R-K$ and $J-K$ is shown in Figure 1, along with their suggested $R-K \geq 5.3$ selection criterion (*dotted lines*). This color space does successfully classify three EROs from the literature with spectroscopic classifications, visible, and NIR photometry: HR 10 (Graham & Dey 1996), LBDS 53W091 (Spinrad et al. 1997), and Cl 0939+4713B (Soifer et al. 1999) (*open triangles*). It is possible, however, that galaxies with a mix of old stars and dusty star formation could fall into either class on this diagram. For example, Hall et al. (2001) found evidence of this in their study of EROs associated with radio-loud quasars, in which objects best fitted by star formation and dust still had relatively blue $J-K$ colors. Of the nine DMS EROs shown in the figure, seven have colors consistent with elliptical galaxies and two are consistent with dusty starbursts. However, six of the EROs fall within 1 σ of the dividing line between these two classes, and therefore either interpretation is consistent with the photometry.

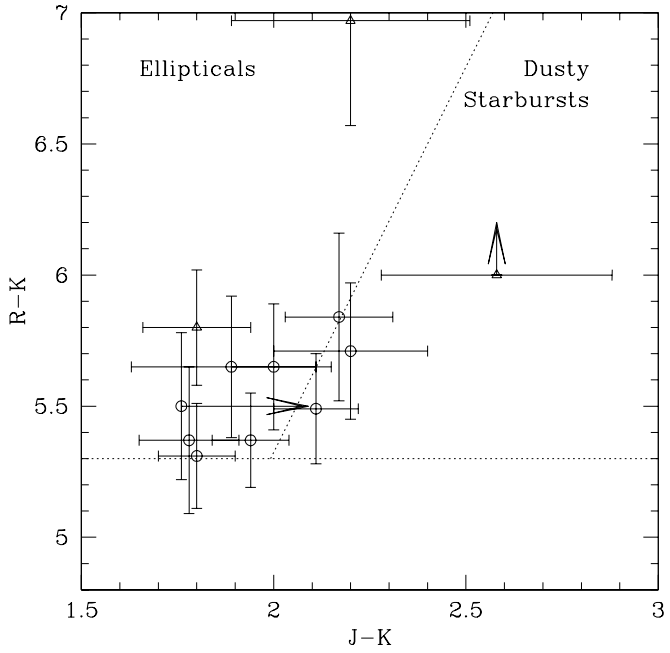

FIG. 1.—$J-K$ vs. $R-K$ diagram for EROs, showing nine EROs (*open circles*) and three EROs from the literature (*open triangles*). The model by Pozzetti & Mannucci (2000) to discriminate between elliptical galaxies and dusty starbursts nearly equally divides (*dotted line*) the ERO sample.

4.2. *SED Template Fits*

Photometric redshifts with SED template fits are one way to expand on simpler color discrimination techniques and solve for both the object redshift and spectrophotometric galaxy type. Photometric redshifts that fit SED templates to photometric data rely on three pieces of information: a template SED for the source object, the relative transmission of the system (filter, detector, and optics) in each band, and a measurement of the source brightness in that band. Of these three quantities, the system transmission profile should in principle be the best-known and the true galaxy SED the

TABLE 1

PHOTOMETRY OF THE ERO SAMPLE

ERO	FIELD	U[a]	B[a]	V	R	I_{75}	I_{86}	J	H	K
1.....	01WC	23.0	23.8	23.440 (0.233)	22.935 (0.266)	22.904 (0.343)	21.603 (0.138)	19.377 (0.077)	18.325 (0.069)	17.376 (0.083)
2.....	01WC150W	23.0	23.8	23.5[a]	23.258 (0.301)	22.5[a]	21.826 (0.178)	19.590 (0.096)	18.622 (0.093)	17.417 (0.098)
3.....	01WC150W	23.0	23.8	23.5[a]	22.506 (0.159)	21.710 (0.113)	20.790 (0.069)	19.072 (0.064)	18.228 (0.068)	17.132 (0.075)
4.....	01WC150W	23.0	23.8	23.884 (0.323)	22.591 (0.177)	21.929 (0.136)	20.794 (0.068)	19.079 (0.061)	18.266 (0.062)	17.279 (0.082)
5.....	10EC	22.7	23.6	23.404 (0.251)	22.949 (0.241)	22.877 (0.372)	21.133 (0.094)	19.2[a]	18.343 (0.114)	17.445 (0.139)
6.....	10EC	22.7	23.6	23.3[a]	22.906 (0.247)	21.704 (0.130)	21.153 (0.094)	19.139 (0.236)	18.433 (0.113)	17.252 (0.098)
7.....	14NC150E	22.6	23.8	23.732 (0.342)	22.902 (0.260)	21.758 (0.157)	20.929 (0.177)	19.307 (0.085)	18.335 (0.081)	17.532 (0.104)
8.....	14NC150E	22.6	23.8	23.4[a]	22.727 (0.197)	22.3[a]	20.849 (0.108)	19.355 (0.084)	18.293 (0.078)	17.236 (0.078)
9.....	CF3	23.0[a]	23.8[a]	23.5[a]	22.971 (0.223)	22.385 (0.223)	21.352 (0.117)	19.464 (0.155)	18.674 (0.145)	17.261 (0.126)

[a] The 3 σ upper limit.

TABLE 2

ERO Photometric Redshifts

		Coleman et al.				Elliptical			Starburst		
ERO (1)	Field (2)	z (3)	χ^2_ν (4)	A_V (5)	SED (6)	z (7)	χ^2_ν (8)	A_V (9)	z (10)	χ^2_ν (11)	A_V (12)
1.....	01WC	1.19	0.6	1.2	Scd	1.17	1.0	0.4	1.28	1.2	1.2
2.....	01WC150W	1.22	0.2	0.6	Sbc	1.07	0.3	0.4	1.06	0.2	1.0
3.....	01WC150W	0.81	1.3	0.0	E	0.81	1.3	0.2	0.95	0.3	1.2
4.....	01WC150W	0.83	0.8	0.0	E	0.85	1.2	0.2	0.96	0.4	1.0
5.....	10EC	0.90	1.4	0.0	E	0.92	1.5	0.2	1.17	0.9	1.2
6.....	10EC	0.78	1.3	0.2	E	0.80	1.4	0.4	0.91	0.8	1.2
7.....	14NC150E	0.78	0.7	0.0	E	0.78	0.8	0.2	0.79	0.7	0.0
8.....	14NC150E	1.07	1.7	0.4	Sbc	0.84	1.6	0.4	0.98	0.9	1.2
9.....	CF3	1.07	0.7	0.6	Sbc	0.90	0.9	0.4	1.00	0.4	1.2

Note.—Photometric results for the ERO sample. Cols. (1) and (2): number and field for each ERO as in Table 1; cols. (3)–(6): best-fit photometric redshift, χ^2_ν, A_V, and SED for the Coleman et al. (1980) SED template; cols. (7)–(9): best-fit parameters for a GISSEL98 elliptical galaxy; cols. (10)–(12): best-fit parameters for a GISSEL98 starburst model.

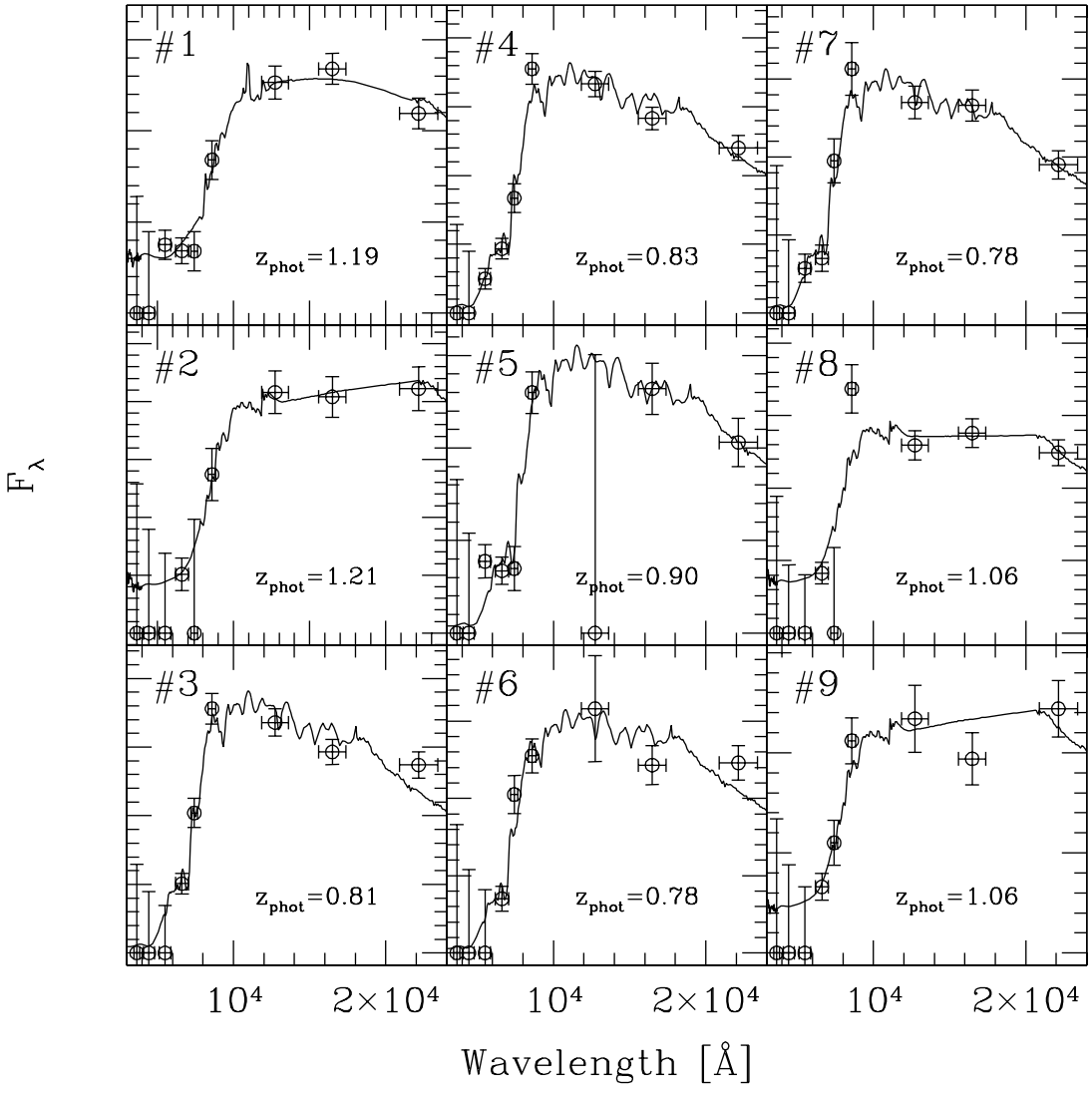

Fig. 2.—Best-fitting SEDs for the EROs. Each panel contains the observed photometry for an ERO from Table 1 (*circles with error bars*) and the best-fit empirical galaxy template (*solid line*) from Coleman, Wu, & Weedman (1980).

most uncertain. The templates used in photometric redshift codes are either empirical SEDs, such as the set compiled by Coleman, Wu, & Weedman (1980), or spectral synthesis templates, such as those based on the Bruzual & Charlot evolutionary code (e.g., GISSEL98; Bruzual & Charlot 1993).

Photometric redshift codes are most accurate in the $z \sim 1$–2 range when NIR photometry is available (e.g., Gwyn 1995; Bolzonella, Miralles, & Pelló 2000). At this range of redshifts the strongest spectral feature, the 4000 Å break, has shifted into the NIR region, and the Lyman continuum has not yet shifted into the ground-based U-filter bandpass. Using mock galaxy catalogs produced with HYPERZ (Bolzonella et al. 2000), I measured the accuracy of the photometric redshift measurements for a $K \leq 18$ mag galaxy sample with the same magnitude limits and noise properties as this survey in all nine filters. For a uniform distribution in redshifts, the scatter is $\sigma_z = 0.08$. The scatter for galaxies with $0.8 \leq z \leq 2$ is $\sigma_z = 0.1$, compared with $\sigma_z = 0.3$ for the same sample if only $UBVRI_{75}I_{86}$ photometry is available. The accuracy of photometric redshifts and the associated best-fit templates depends on photometric quality, as well as the number of filters. While the EROs are all expected to be at $z \geq 0.8$ because of their $R-K$ colors, they are often undetected in several filters (none are detected in U or B), and the photometric uncertainties in the remaining filters are generally greater than 0.1 mag. The larger the photometric errors, the less well constrained the best-fit redshift and particularly the best-fit galaxy template.

The empirical galaxy templates in HYPERZ are from Coleman et al. (1980) and represent the local galaxy population. The GISSEL98 galaxy templates are the 1998 update of the spectral synthesis models described by Bruzual & Charlot (1993). All the models have solar metallicity and a Miller & Scalo (1979) initial mass function. Each model corresponds to a different present-day spectrophotometric galaxy type. The elliptical template has all star formation occurring at high redshift and thus represents classic passive luminosity evolution. The burst model represents the opposite extreme, with significant recent star formation. The remaining galaxy types are represented by exponentially decaying star formation with different e-folding timescales.

I used HYPERZ to find the best-fit empirical galaxy template, GISSEL98 elliptical template, and GISSEL98 starburst templates for each of the EROs listed in Table 1. The basic operation of this code is to take a series of input galaxy templates, vary the redshift and amount of reddening, and solve for the best combination of these quantities that match an input catalog of photometric measurements or upper limits. For these model fits I adopted the Calzetti et al. (2000) reddening law. While there are a large number of filters predefined in HYPERZ, the DMS I_{75} and I_{86} filters are not included. Because of the importance of the system transmission profiles in each band, I added the profiles of the DMS filters from Hall et al. (1996a), which include the detector response, and scans of the J, H, and K filters from TIFKAM, which I convolved by a measurement of the atmospheric transmission at Kitt Peak.

In all cases the photometric redshift predictions of the three fits shown in Table 2 are similar. One feature of the SED fits to these EROs is that on average the best-fit elliptical template has a lower photometric redshift than the best starburst template. This is because the dominant break in the SED of elliptical galaxies is at 4000 Å, while the closest spectral break in starburst galaxies is the Balmer continuum at 3650 Å. The rms scatter in the photometric redshift prediction for these three fits is $\sigma_z < 0.1$. The photometric redshifts are thus quite robust and show clearly that these EROs are $z \geq 0.8$ galaxies. The relative quality of the three SED fits is comparable, with the difference between the fits $\Delta\chi^2_\nu \leq 1$. These galaxies cannot therefore be reliably classified as either elliptical galaxies or dusty starbursts because of the large photometric errors. Most of the best fits with the Coleman et al. (1980) empirical SEDs, shown in Figure 2, are those based on the elliptical template with no dust or those based on spirals with some dust. These fits suggest that most EROs are elliptical galaxies, although old stellar populations at $z \sim 1$ are on order half the age of old stellar populations at $z \sim 0$, and thus this empirical SED may not be an accurate representation of $z \sim 1$ elliptical galaxies. The GISSEL98 models do take the change in the age of the stellar population with redshift into account. The GISSEL98 elliptical templates fit the data with only a small amount of extinction, while the starburst models require on average $A_V = 1$ mag.

5. DISCUSSION

The reported surface density of EROs has a large dispersion. Elston et al. (1988) found two galaxies with $R-K \geq 5$ and $K \leq 18$ mag in 10 arcmin^2 for a surface density of 0.2 arcmin^{-2}. Figure 1 of Thompson et al. (1999) shows they found seven of these objects for a surface density of 0.05 arcmin^{-2}. Daddi et al. (2000) surveyed 700 arcmin^2 and derived a surface density of 0.08 arcmin^{-2} for $R-K \geq 5$ and $K \leq 18$ mag. Their study also showed that EROs are clustered, which helps to explain the dispersion in measurements of the surface density. In this survey I have identified nine EROs with $R-K \geq 5.3$ and $K \leq 18$ mag, which corresponds to a surface density of $0.049^{+0.022}_{-0.016}$ arcmin^{-2}, where these uncertainties correspond to only the 1 σ confidence limits (Gehrels 1986). This surface density is nearly a factor of 2 higher than the surface density of 0.027 arcmin^{-2} found by Daddi et al. (2000) for $R-K \geq 5.3$ and $K \leq 18$ mag (see Table 3), although based on Poisson statistics these measurements are marginally consistent at the 1 σ level.

In addition to the random errors due to counting statistics, Eddington bias and light lost outside the $R = 2''$ aperture could systematically lower and raise the measured surface density, respectively. Eddington bias is important near the detection limit when objects with a steep number-magnitude relation are preferentially scattered into the sample and artificially enhance the observed space density. Based on the surface density versus magnitude measurements published by Daddi et al. (2000), the slope of the ERO number-magnitude relation (for $R-K \geq 5.3$) is $\alpha \sim 0.9$ at $K \sim 18$ mag. The correction for the Eddington bias is $\sim 2.65\sigma^2\alpha^2$, and for a mean photometric uncertainty of $\sigma \sim 0.1$ the surface density may be overestimated by approximately 2%. If the slope is a factor of 2 steeper, the overestimate is still less than 10%. A more significant potential source of error arises if the EROs are large galaxies and an $R = 2''$ aperture misses some fraction of their light. Then the surface density has been underestimated as the photometric scale effectively assigns them too faint a magnitude, thus the surface density at $K = 18$ mag is really the surface

TABLE 3

ERO Surface Density

K Range (mag) (1)	Σ_K (all galaxies) (arcmin^2) (2)	$z \geq 0.8$ (Percent) (3)	Σ_K ($z \geq 0.8$) (arcmin^2) (4)	$\Sigma_{\rm ERO}$ (arcmin^2) (5)	$\Sigma_{\rm ERO}$ (arcmin^2) (6)
16–18.....	1.67	<1	<0.017	0.05	0.027
18–19.....	3.33	<10	<0.33	...	0.27

Note.—Surface density of EROs with $R-K \geq 5.3$. Col. (1): K-magnitude ranges; col. (2): surface density of all galaxies in this magnitude range from Martini (2001); col. (3): percent of all galaxies at $z \geq 0.8$ in these magnitude ranges from the hierarchical galaxy model prediction of Kauffmann & Charlot (1998); col. (4): expected surface density of galaxies at $z \geq 0.8$; col. (5): measured surface density of EROs, which are lower limits to the surface density of all $z \geq 0.8$ galaxies, from this paper; col. (6): same as col. (5), but from Daddi et al. (2000). The measurements in these columns are higher than the hierarchical model predictions for $K \leq 18$ mag, but are consistent with this model for $18 < K < 19$ mag.

density at $K = 18 - \delta m$ mag. The increase in surface density scales as $10^{\alpha \delta m}$, where, for example, $\delta m = 0.2$ ($r_h = 1''$ for an exponential or $r^{1/4}$ profile) corresponds to an increase of 50%, although a significant contribution from such large EROs appears to be ruled out by observations (Moriondo et al. 2000).

While clustering will not change the true mean surface density, it will increase the possible variation from survey to survey over the pure Poisson uncertainties quoted above. The DMS EROs are clearly strongly clustered as, for example, five of these objects are in one of the subfields in field 01W (01WC, 01WC150W, and CF3), only 20% of the total area with NIR data. The rms number counts of EROs in the DMS are $\sigma = 0.85$, compared with the Poisson value of $\sigma_{\rm Pois} = 0.67$ for a surface density of 0.05 arcmin^2 and an average area per field of 9 arcmin^2. If I adopt the correlation amplitude $A = 0.024$ from Daddi et al. (2000) for $R-K \geq 5$ and $K \leq 18$ mag (they had insufficient statistics to measure this quantity at $R-K \geq 5.3$), the predicted rms counts (Roche et al. 1999; Daddi et al. 2000) are $\sigma = 0.75$. The clustering signal in this survey may be exaggerated by variations in the field-to-field sensitivity.

The high surface density of EROs in this and other surveys provides a constraint for passive evolution and hierarchical galaxy formation models. Hierarchical models predict relatively few large, bright galaxies at $z \sim 1$ as most of these galaxies assemble at $z < 1$. In a simple test of hierarchical galaxy formation, Kauffmann & Charlot (1998) predicted that less that 1% of all galaxies with $16 < K < 18$ mag are at $z \geq 0.8$ and $\sim$10% of galaxies with $18 < K < 19$ mag are at $z \geq 0.8$ (see their Fig. 4). Measurements of the K number-magnitude relation (e.g., Minezaki et al. 1998; Martini 2001) show the galaxy surface density is $\sim$1.7 arcmin^{-2} for galaxies with $16 < K < 18$ mag and $\sim$3.3 arcmin^{-2} for galaxies with $18 < K < 19$ mag. As all EROs with spectroscopic or photometric redshifts are at $z \geq 0.8$, the surface density of EROs can be taken as a lower limit to the surface density of all $z \geq 0.8$ galaxies to test the Kauffmann & Charlot (1998) prediction of hierarchical galaxy formation. Their predicted fraction of galaxies at $z \geq 0.8$ implies that the surface density of EROs should be less than 0.017 arcmin^{-2} for $16 < K < 18$ mag, in conflict with the higher value I measure and the value measured by Daddi et al. (2000). According the passive evolution model in Kauffmann & Charlot (1998), $\sim$50% of all galaxies at $K \leq 18$ mag are at $z \geq 0.8$, which corresponds to over an order of magnitude greater surface density for all $z \geq 0.8$ galaxies than the ERO surface density presented here, even if the ERO surface density has been underestimated by as much as 50% because of lost light in the aperture.

The ERO surface density I measure and the measurement of Daddi et al. (2000) are still consistent with the results of K-selected spectroscopic and photometric redshift surveys (Songaila et al. 1994; Cowie et al. 1996; Fontana et al. 1999), which have found a somewhat higher surface density of $z \geq 0.8$ galaxies than the hierarchical model predictions. The cosmic variance between different redshift and ERO surveys should be large, given the clustering of EROs. The redshift distribution from a spectroscopic survey is also most likely to be incomplete for the reddest and highest-redshift galaxies and could underestimate the $z \sim 1$ contribution.

EROs provide such a good means to test the hierarchical galaxy formation model because their surface density is greater than the predicted surface density of all $z \geq 0.8$ galaxies and they are only a lower limit on the total $z \geq 0.8$ galaxy population in a K-selected galaxy survey. From the discussion of the systematic uncertainties in the surface density above, the overestimate due to Eddington bias is less significant than an underestimate due to lost galaxy light, and therefore 0.05 arcmin^{-2} may be a lower limit to the true ERO surface density. The surface density is therefore nearly a factor of 3 higher than the predicted surface density of all $z \geq 0.8$ galaxies. Two other effects could bring the ERO surface density into better agreement with the hierarchical prediction, either by decreasing the observed number of EROs or increasing their expected number. Some fraction of EROs appears to be dusty starburst galaxies rather than old elliptical galaxies. While this fraction is very likely less than 50% based on the colors of these EROs and on spectroscopic observations of ERO samples from the literature (Cimatti et al. 1999; Cohen et al. 1999), decreasing the surface density from this survey by a factor of 2 still yields a higher surface density of objects than the hierarchical model. A more important effect, however, is that the current model predictions from Kauffmann & Charlot (1998) are for an $\Omega_M = 1$ universe. In a flat, Λ-dominated universe, which appears to be the best-fit cosmological model, the comoving volume element versus redshift is larger than in a flat, matter-dominated universe. For example, at $z = 1$ a given surface area on the sky corresponds to a factor of 2.8 $(h_M/h_\Lambda)^3$ more comoving volume in an $\Omega_M = 0.3$, $\Omega_\Lambda = 0.7$ universe than in an $\Omega_M = 1$, $\Omega_\Lambda = 0$ universe. The volume per unit area on the sky is greater and

implies a larger surface density of high-redshift objects than that implied by the matter-dominated model considered by Kauffmann & Charlot (1998). The growth factor is also larger at fixed redshift in a Λ-dominated universe than in an $\Omega_M = 1$ model, which implies that more large structures have formed and consequently there are a larger space density and surface density of bright galaxies. The increase in surface density due to the change from a matter-dominated to a Λ-dominated universe is partially offset, however, by the increase in the luminosity distance.

In this paper I have presented a new measurement of the ERO surface density and used photometric redshifts to show these objects are galaxies at $z \geq 0.8$. The surface density of EROs is a lower limit to the total $z \geq 0.8$ surface density, yet it is still a factor of 3 larger than the hierarchical galaxy formation model prediction for a matter-dominated universe. Hierarchical galaxy formation in a Λ-dominated universe, rather than a matter-dominated universe, could account for this discrepancy.

I would like to thank Darren DePoy, Patrick Osmer, and David Weinberg for helpful discussions and comments on this manuscript. In addition, helpful comments from an anonymous referee have improved and clarified this presentation. I also acknowledge the staff of the MDM Observatory. I was supported in part by a Presidential Fellowship from Ohio State University and received additional travel and other support from a PEGS grant and the Department of Astronomy at Ohio State University. TIFKAM was funded by Ohio State University, the MDM consortium, MIT, and NSF grant AST 96-05012. NOAO and USNO paid for the development of the ALADDIN arrays and contributed the array currently in use in TIFKAM.

REFERENCES

Baugh, C. M., Cole, S., Frenk, C. S., & Lacey, C. G. 1998, ApJ, 498, 504
Bolzonella, M., Miralles, J.-M., & Pelló, R. 2000, A&A, 363, 476
Bruzual, A. G., & Charlot, S. 1993, ApJ, 405, 538
Bruzual, G., & Kron, R. G. 1980, ApJ, 241, 25
Calzetti, D., Armus, L., Bohlin, R. C., Kinney, A. L., Koornneef, J., & Storchi-Bergmann, T. 2000, ApJ, 533, 682
Cimatti, A., Andreani, P., Rottgering, H., & Tilanus, R. 1998, Nature, 392, 895
Cimatti, A., et al. 1999, A&A, 352, L45
Cohen, J. G., Blandford, R., Hogg, D. W., Pahre, M. A., & Shapbell, P. L. 1999, ApJ, 512, 30
Coleman, D. G., Wu, C. C., & Weedman, D. W. 1980, ApJS, 43, 393
Cowie, L. L., Songaila, A., Hu, E. M., & Cohen, J. G. 1996, AJ, 112, 839
Daddi, E., Cimatti, A., Pozzetti, L., Hoekstra, H., Röttgering, H. J. A., Renzini, A., Zamorani, G., & Mannucci, F. 2000, A&A, 361, 535
Dey, A., Graham, J. R., Ivison, R. J., Smail, I., Wright, G. S., & Liu, M. C. 1999, ApJ, 519, 610
Elston, R., Rieke, G. H., & Rieke, M. J. 1988, ApJ, 331, L77
Elston, R., Rieke, M. J., & Rieke, G. H. 1989, ApJ, 341, 80
Fontana, A., Menci, N., D'Odorico, S., Giallongo, E., Poli, F., Cristiani, S., Moorwood, A., & Saracco, P. 1999, MNRAS, 310, L27
Gardner, J. P., Sharples, R. M., Frenk, C. S., & Carrasco, B. E. 1997, ApJ, 480, L99
Gehrels, N. 1986, ApJ, 303, 336
Graham, J. R., & Dey, A. 1996, ApJ, 471, 720
Gwyn, S. D. J. 1995, M.Sc. thesis, Univ. Victoria
Hall, P. B., Osmer, P. S., Green, R. F., Porter, A. C., & Warren, S. J. 1996a, ApJS, 104, 185
———. 1996b, ApJ, 471, 1073
Hall, P. B., et al. 2001, AJ, in press
Hu, E., & Ridgway, S. 1994, AJ, 107, 1303
Kauffmann, G., & Charlot, S. 1998, MNRAS, 294, 705
Kennefick, J. D., Osmer, P. S., Hall, P. B., & Green, R. F. 1997, AJ, 114, 2269
Lacey, C., Guiderdoni, B., Rocca-Volmerange, B., & Silk, J. 1993, ApJ, 402, 15
Liu, C. T., Green, R. F., Hall, P. B., & Osmer, P. S. 1998, AJ, 116, 1082
Martini, P. 2001, AJ, 121, 598
Martini, P., & Osmer, P. S. 1998, AJ, 116, 2513
McCarthy, P. J., Persson, S. E., & West, S. C. 1992, ApJ, 386, 52
Miller, G. E., & Scalo, J. M. 1979, ApJS, 41, 513
Minezaki, T., Kobayashi, Y., Yoshii, Y., & Peterson, B. A. 1998, ApJ, 494, 111
Moriondo, G., Cimatti, A., & Daddi, E. 2000, A&A, 364, 26
Osmer, P. S., Kennefick, J. D., Hall, P. B., & Green, R. F. 1998, ApJS, 119, 189
Persson, S. E., McCarthy, P. J., Dressler, A., & Matthews, K. 1993, in The Evolution of Galaxies and Their Environment, ed. M. Shull & H. Thronson (NASA CP-3190) (Washington: GPO), 78
Pozzetti, L., & Mannucci, F. 2000, MNRAS, 317, L17
Roche, N., Eales, S., Hippelein, H., & Willott, C. J. 1999, MNRAS, 306, 538
Scodeggio, M., & Silva, D. R. 2000, A&A, 359, 953
Soifer, B. T., Matthews, K., Neugebauer, G., Armus, L., Cohen, J. G., Persson, E., & Smail, I. 1999, AJ, 118, 2065
Songaila, A., Cowie, L. L., Hu, E. M., & Gardner, J. P. 1994, ApJS, 94, 461
Spinrad, H., Dey, A., Stern, D., Dunlop, J., Peacock, J., Jimenez, R., & Windhorst, R. 1997, ApJ, 484, 581
Steidel, C. C., Adelberger, K. L., Giavalisco, M., Dickinson, M., & Pettini, M. 1999, ApJ, 519, 1
Steidel, C. C., Giavalisco, M., Pettini, M., Dickinson, M., & Adelberger, K. L. 1996, ApJ, 462, L17
Steidel, C. C., & Hamilton, D. 1993, AJ, 105, 2017
Thompson, D., et al. 1999, ApJ, 523, 100
Tinsley, B. M. 1977, ApJ, 211, 621
White, S. D. M., & Frenk, C. S. 1991, ApJ, 379, 52
White, S. D. M., & Rees, M. J. 1978, MNRAS, 183, 341
Yan, L., McCarthy, P. J., Weymann, R. J., Malkan, M. A., Teplitz, H. I., Storrie-Lombardi, L. J., Smith, M., & Dressler, A. 2000, AJ, 120, 575